Chinese Chemical Letters 34 (2023) 107798

Contents lists available at ScienceDirect

Chinese Chemical Letters

journal homepage: www.elsevier.com/locate/cclet

A unique Janus PdZn-Co catalyst for enhanced photocatalytic syngas production from CO_2 and H_2O

Dongxue Zhou[a,b,1], Xiangdong Xue[a,1], Qingjie Luan[a,b], Liguo Zhang[a,b], Baozhen Li[a,b], Xing Wang[a,b], Wenjun Dong[a,b,*], Ge Wang[a,*], Changmin Hou[c]

[a] Beijing Advanced Innovation Center for Materials Genome Engineering, Beijing Key Laboratory of Function Materials for Molecule & Structure Construction, School of Materials Science and Engineering, University of Science and Technology Beijing, Beijing 100083, China
[b] Shunde Graduate School of University of Science and Technology Beijing, Foshan 528399, China
[c] State Key Laboratory of Inorganic Synthesis & Preparative Chemistry, College of Chemistry, Jilin University, Changchun 130012, China

ARTICLE INFO

Article history:
Received 9 August 2022
Accepted 1 September 2022
Available online 9 September 2022

Keywords:
PdZn@C catalyst
Janus structure
Charge redistribution
Absorption modulation
Photocatalyst

ABSTRACT

The development of excellent catalyst to achieve photocatalytic syngas production from CO_2 and H_2O is a prospective and sustainable strategy to alleviate environment and energy crisis. In this study, a unique Janus PdZn-Co catalyst is prepared by annealed the Pd/IRMOF-3(Co, Zn) precursor. Due to the strong interaction, the electron transfers from PdZn terminal to Co terminal in the Janus structure. The electron-received Co terminal facilitates Co sites coordinate with the electrophilic C atom of CO_2 and the electron-donated PdZn center is easier to coordinate with nucleophilic O atoms of H_2O or C=O bonds. The charge redistribution enhances the absorption of CO_2 and H_2O, which promotes H_2 evolution and CO production. In addition, the carbon shell effectively suppresses the metal core agglomeration and facilitates the electron transmission from photosensitizer to metallic active sites. Meanwhile, the ratio of CO/H_2 can be regulated (~3:1 to 2:1) by adjusting the proportion of Co and PdZn. The Janus structure and graphite carbon synergistically play a profound impact on improving the photocatalytic performance. The optimized PdZn-Co catalyst exhibits a superior photocatalytic CO production rate (20.03 μmol/h) and the H_2 generation rate (9.90 μmol/h) with a ratio of $CO/H_2 = 2.02$.

Syngas (a mixture of CO and H_2), as an important chemical raw gas, has drawn extensive attention for hydrocarbons, alcohols or other fine chemicals production by Fischer-Tropsch process [1–4]. Usually, syngas is produced by gasification of fossil fuels under high temperature and pressure conditions in industry. However, the required high energy consumption and harsh reaction condition exerts much pressure for environment and energy, restricting the sustainable development of economy [5]. In recent years, photo- and electro- catalytic reduction of CO_2 and H_2O to produce syngas have drawn a widespread interest in catalytic field [6–10]. Further, CO_2 and H_2O as feedstock can effectively alleviate the energy crisis and environmental pollution. Compared with electrocatalytic CO_2 and H_2O reduction, the photocatalytic syngas production strategy is directly utilizing the exhaustible solar energy to achieve CO_2 and H_2O reduction into syngas (CO and H_2) with photocatalyst [4,11,12]. Up to now, efficient photocatalysts for CO_2 and H_2O reduction, including Vs-$CuIn_5S_8$ [13], CoN [14], $Co(OH)_2$ [15], $ZnCo_2O_4$ [16], $CuCo_2O_4$ [17], Ni MOFs [18], have been extensively exploit. Moreover, the syngas with different molar ratios of $CO:H_2$ (1:1, 1:2 and 1:3) can be successfully tuned for practical chemicals production. For example, a syngas ratio of 1:3 ($CO:H_2$) is selected as the raw material to synthesize ammonia, and 1:1 ratio ($CO:H_2$) syngas is required in oxo-alcohols production. Hence, it is essential to design a novel photocatalyst with high activity and tunable CO/H_2 syngas ratios output.

In recent years, multifarious photocatalysts have been exploited to pursue the superior property for CO_2 and H_2O reduction. Cobalt based catalysts such as metallic Co [19], Co_3O_4 [20–22], CoN [14], single-atom Co [23], $NiCo_2O_4$ [24], $CoWO_4$ [25] and Co–M [26] alloy exhibit excellent photocatalytic CO_2 reduction and H_2 evolution performance. Co sites can accelerate charge migration, active CO_2 and H_2O molecules and promote surface reduction kinetics. For example, metallic Co–C catalyst [19], in which Co served as the active sites and the graphite carbon coating on the metal acted as the electron transmission medium, showed excellent catalytic performance to reduce CO_2 and H_2O under visible-light irradiation. Hexagonal-shaped Co_3O_4 platelets with plentiful {112}

* Corresponding authors.
E-mail addresses: wdong@ustb.edu.cn (W. Dong), gewang@ustb.edu.cn (G. Wang).
[1] These authors contributed equally to this work.

https://doi.org/10.1016/j.cclet.2022.107798
1001-8417/

exposed facets optimized the solar-driven CO_2 and H_2O conversion activity [21]. The fully exposed {112} facets of Co_3O_4 promoted the adsorption behavior of CO_2 and H_2O, thus resulting in high catalytic activity. The optimized Co_3O_4 catalyst exhibits a CO production rates of 2003 μmol g^{-1} h^{-1} and H_2 evolution rate of 595 μmol g^{-1} h^{-1}, with a ratio of is 3.37:1 (CO/H_2). $CoWO_4$ catalysts with high crystallinity showed a uniform mesoporous structure, which can provide high surface area and plentiful active sites for CO_2 adsorption. Meanwhile, $CoWO_4$ acted as electron capturer to accelerate the separation/transfer of photoinduced carriers, thus greatly boosting the CO_2 reduction efficiency [25]. The Co-based catalysts show favorable performance, whereas the tunable CO/H_2 ratio of syngas remains a great challenge.

Herein, a Janus PdZn-Co heterostructure catalyst was prepared *via* pyrolysis of Pd/IRMOF-3(Co, Zn), which exhibited superior photocatalytic property and a controllable syngas (CO/H_2) ratio (~3:1 to 2:1). During the pyrolysis procedure, the Zn^{2+} in the IRMOF-3 host and Pd^{2+} anchored on the -NH_2 group of MOFs were reduced into intermetallic PdZn, simultaneously, the Co^{2+} substituted Zn in MOFs were reduced to metallic Co in H_2. Due to the lattices incompatibility, the tetragonal PdZn and cubic Co formed the Janus structure. Further, ligands of MOFs were converted into carbon shell covering on the surface of Janus PdZn-Co, which promoted the electron transmission from the photosensitizer to metallic active sites. DFT calculation results demonstrate the electron transfers from PdZn terminal to Co terminal in the Janus structure. The electron-received Co terminal facilitates Co sites coordinate with the electrophilic C atom of CO_2 and the electron-donated PdZn center is easier to coordinate with nucleophilic O atoms of H_2O or C=O bonds. The charge redistribution enhances the absorption of CO_2 and H_2O, promotes photocatalytic H_2 evolution and CO_2 reduction. Moreover, the ratio of CO/H_2 is controlled through regulating the proportion of PdZn and Co terminals in the Janus catalyst. The design of novel Janus catalyst provides more opportunities for developing high-efficiency sunlight-driven catalytic applications.

The synthesis process of Janus PdZn-Co catalyst is schematically shown in Fig. S1 (Supporting information). XRD result demonstrates intermetallic PdZn and metallic Co coexist in the PdZn-Co catalysts (Fig. 1a). The 44.2°, 51.5° and 75.7° characteristic peaks belong to the (111), (200), (220) crystal planes of the cubic α-Co (JCPDS No. 89-4307)[28]. The diffraction peaks at 41.2°, 44.1°, 64.2°, 72.9° and 79.2° can be indexed to (111), (200), (112), (202) and (311) planes of tetragonal PdZn (JCPDS No. 65-9523). The intensity of the (111) peak corresponded to intermetallic PdZn increases significantly with the Pd content increase (Fig. 1b). The as prepared PdZn-Co nanoparticle is ~50 nm in diameter with a metallic core and carbon shell (Fig. 1c). A clear PdZn-Co interface confirms the distal separation of the Janus structure (Fig. 1d). The element mapping indicates the Co, Zn and Pd elements are uniformly dispersed into two terminals of PdZn-Co. One side of the nanoparticle is mainly distributed with Co elements and the other side is mainly concentrated with Pd and Zn element. The interplanar spacings of Co terminal are 0.18 and 0.20 nm, which correspond to the cubic α-Co (200) and (111) facets (Fig. 1e). The lattice fringe of 0.20 nm and 0.22 nm consistent with intermetallic PdZn (200) and (111) facets (Fig. 1f). A carbon shell can be clearly observed on the surface of metallic core (Fig. S4 in Supporting information). The lattice fringes of 3.4 Å belongs to the (002) plane of graphene carbon. The exist of carbon shell can effectively suppress the metal core agglomeration.

To reveal the electronic structures of Janus structure, XPS analysis are carried out over the PdZn-Co, Co@C and PdZn@C (Fig. 2). The Co 2p spectrum can be deconvoluted into two spinorbit doublets and two satellite peaks (at 784.88 and 803.30 eV, donated as "Sat.") (Fig. 2b). Compared with the Co@C, the first doublet peaks belonged to Co^0 for PdZn-Co shift to the low binding energy [from

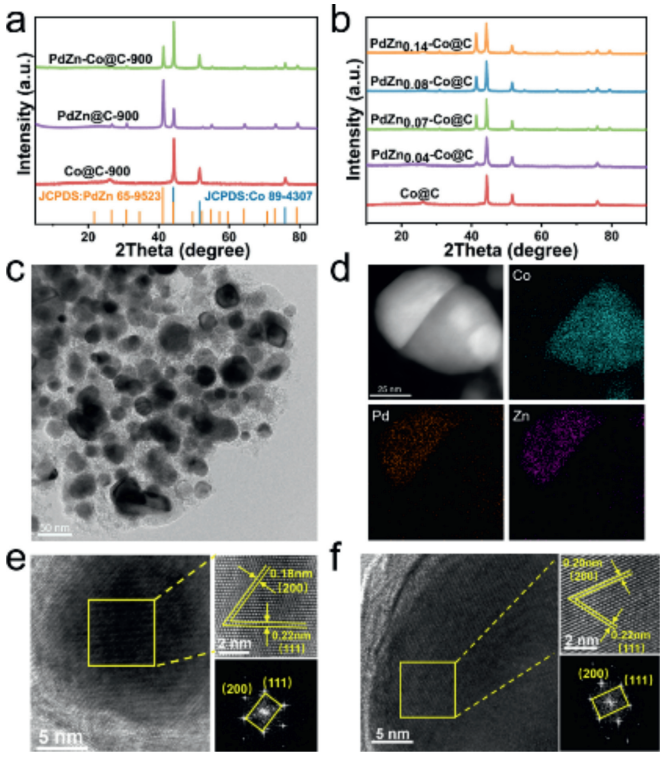

Fig. 1. (a) XRD patterns with different samples, (b) XRD patterns of PdZn-Co with different Pd content, (c) TEM image, (d) element mapping and (e, f) HRTEM image of PdZn-Co.

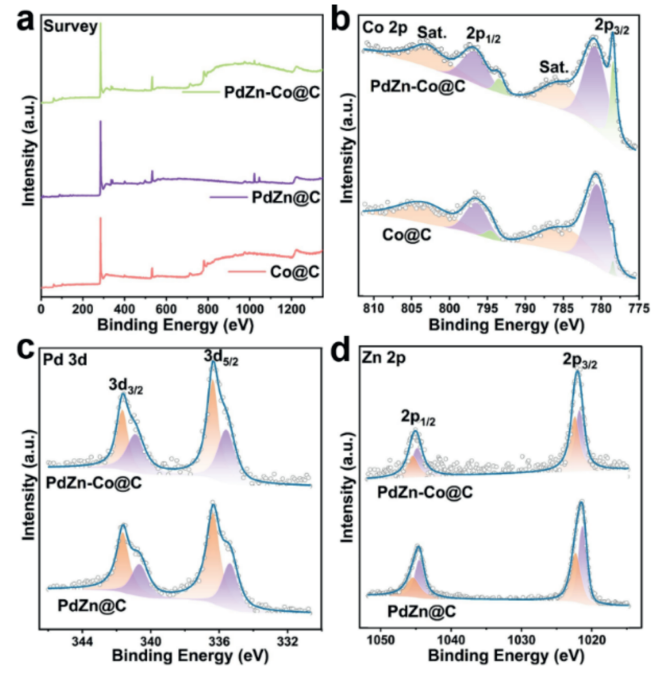

Fig. 2. XPS spectra. (a) Survey, (b) Co 2p, (c) Zn 2p and (d) Pd 3d.

(778.46 $2p_{3/2}$ and 794.55 eV $2p_{1/2}$) to (778.43 $2p_{3/2}$ and 793.44 eV $2p_{1/2}$)], while the second doublet peaks assigned to Co^{2+} shift to the high binding energy [from (780.49 $2p_{3/2}$ and 796.42 eV $2p_{1/2}$) to (780.75 eV $2p_{3/2}$ and 796.63 eV $2p_{1/2}$)], which confirming the strong election interaction between PdZn and Co [25,26]. For the high resolution Pd 3d region for PdZn-Co (Fig. 2c), the two peaks for the Pd $3d_{3/2}$ and Pd $3d_{5/2}$ electrons could be deconvoluted into

two pairs of doublets. The first doublet peaks belonged to metallic Pd for PdZn-Co (340.91 and 335.59 eV) are remarkably positive than that of PdZn@C (Pd 340.66 and 335.37 eV). The second doublet peaks belonged to PdZn (341.66 and 336.37 eV) are also positive than that of PdZn@C (Pd 341.64 and 336.35 eV). Similar as Pd 3d spectrum, the peaks of Zn 2p also shifted to the high binding energy [from (1021.33 and 1022.33 eV) to (1021.77 and 1022.41 eV)], suggesting the electron transfer from PdZn to metallic Co (Fig. 2d). The charge difference of the Janus catalysts plays a profound influence on the activation of CO_2 and H_2O molecules.

In order to explore the Janus structure evolution, the MOFs precursors are calcined under the different temperature. When the Pd/IRMOF-3(Co, Zn) precursors are annealed at 800 °C, Janus structure tends to form with the Co and PdZn co-existence (Figs. S5a and b in Supporting information). The metallic core is coated with a series of amorphous carbon (Figs. S5c and d in Supporting information). Due to the lattices incompatibility, the tetragonal PdZn and cubic Co formed the Janus structure (Figs. S6 and S7 in Supporting information). At 900 °C calcination, the regular and complete Janus structure (PdZn-Co) forms and some amorphous carbon converts to graphitized carbon. The carbon shell can absorb the sensitizer molecules through π-π interaction [26]. Meanwhile, the carbon shell with porous structure is benefit for small molecules gonging through (Fig. S8 in Supporting information). As is shown in Raman spectra (Fig. S9a in Supporting information), all catalysts display the D bands at about 1346 cm^{-1} and G bands at about 1589 cm^{-1} [27]. The PdZn-Co exhibits the stronger graphitized degree ($I_D/I_G = 2.84$) than PdZn-Co ($I_D/I_G = 3.45$). The graphitization carbon enhances electrical conductivity, which is evidenced by the electrochemical impedance spectroscopy. The EIS circular diameter of PdZn-Co is smaller than that of PdZn-Co, suggesting the graphene carbon can reduce electron transfer resistance to provide high-speed channels for the migration of electrons from the sensitizers to the catalyst (Fig. S9b in Supporting information). As a result, the PdZn-Co exhibit a superior performance than PdZn-Co (Fig. S9c in Supporting information). As further increase the temperature to 1000 °C, due to the Zn volatilization under high temperature, the proportion of PdZn decrease, accompanying with the collapse of Janus structure. The element mapping reveals Pd diffuse into Co phase and Zn content declines sharply (Figs. S5e and f in Supporting information). In short, the unique Janus structure and graphitization carbon synergistically play a profound impact on improvement of the photocatalytic performance.

The photocatalytic CO_2 and H_2O reduction property of the PdZn-Co are evaluated with $[Ru(bpy)_3]Cl_2{\cdot}6H_2O$ photosensitizer in H_2O/TEOA/acetonitrile solution (1:1:3, the total volume = 5 mL). In this system, CO and H_2 as the main gas phase are produced (Fig. 3a). ^1H NMR spectroscopy confirmed that no other liquid phase products are produced (Fig. S10 in Supporting information). The Co@C derived from IRMOF-3(Co, Zn) precursor exhibit a CO production rate of 15.50 μmol/h and H_2 generation rate of 5.28 μmol/h. The PdZn@C derived from Pd/IRMOF-3(Zn) precursor endows a CO production rate of 1.05 μmol/h and H_2 generation rate of 7.46 μmol/h. When the Pd/IRMOF-3(Co, Zn) is annealed, the as-prepared PdZn-Co shows preferable photocatalytic performance. As the proportion of PdZn rise up, the CO formation rates of the $PdZn_1$–Co@C, $PdZn_2$–Co@C, $PdZn_3$–Co@C and $PdZn_4$–Co@C are 17.85 μmol/h, 20.03 μmol/h, 16.28 μmol/h and 13.86 μmol/h. The H_2 evolution rate were 6.43 μmol/h, 9.90 μmol/h, 7.38 μmol/h and 6.56 μmol/h, respectively. Especially, the $PdZn_2$-Co exhibits a superior photocatalytic CO production rate and the H_2 generation rate. The mass content of Co, Pd and Zn are 69.44 wt%, 8.88 wt% and 6.54 wt%, respectively, detected by ICP-OES (Table S1 in Supporting information). Interestingly, the syngas ratio of CO/H_2 can be regulated by adjusting the proportion of Co and PdZn in the catalyst (Fig. 3b). The CO/H_2 ratios over the above catalysts

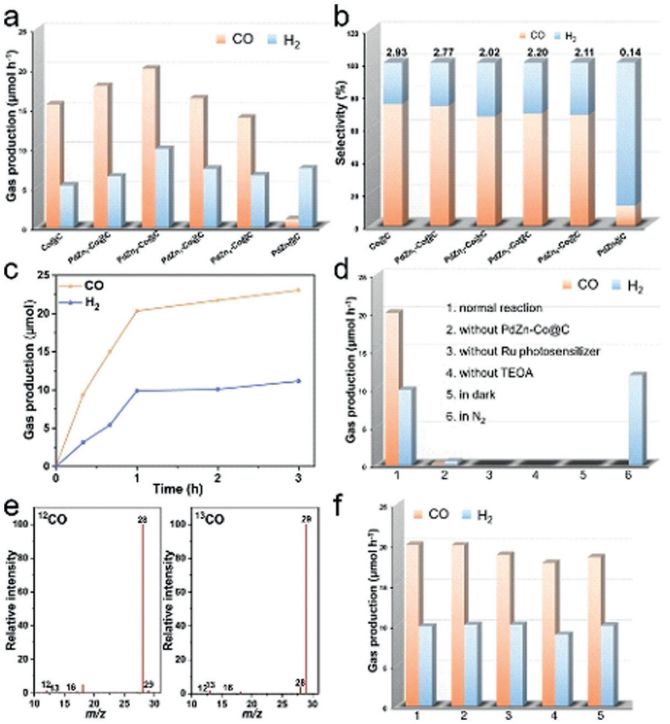

Fig. 3. (a) The photocatalytic performance and (b) the selectivity over different catalysts. (c) Time-dependent CO and H_2 evolution of $PdZn_2$-Co. (d) CO_2 and H_2O photocatalytic performance under various reaction. (e) $^{13}CO_2$ isotope experiment. (f) Recycling test of $PdZn_2$-Co.

are 2.93, 2.77, 2.02, 2.20 and 2.11, respectively. The applicable ratio of CO/H_2 (~3:1 to 2:1) facilitates the subsequent thermochemical conversions to high value-added products. The Janus structure can greatly improve the photocatalytic property and adjust the syngas ratio simultaneously. The CO/H_2 yield increases over time, but the accumulating rate is gradually decreasing, due to the inactivation of the photosensitizer (Fig. 3c). To further illustrate the essential factors for the photocatalytic process, a series of control experiments are conducted (Fig. 3d). In the controlled experiment (2), only trace amount of CO and H_2 are produced without catalysts. No products are generated without Ru photosensitizer in reaction (3), TEOA (4) and incident light (5). The results confirm the reduction are driven by visible-irradiation and the sacrificial agent play a vital role in the reaction. The control experiment with N_2 instead of CO_2 (6) shows that only H_2 is generated, but without any CO production. To trace the origin of produced CO, the isotopic $^{13}CO_2$ is used as the reactant in the reaction [5]. After the photocatalytic reaction, the ^{13}CO are generated and detected by GC–MS, directly confirming the produced CO is originated from CO_2 (Fig. 3e). When no H_2O are added into the reaction system, the production rate of CO and H_2 decline sharply due to H_2O can provide protons to boost CO_2 reduction [28]. The H_2 production drop illustrates the H_2 is originated from H_2O, and H_2 generated in the current system is derived from residual water molecules in the reagent (Table S2 in Supporting information). Besides the superior photocatalytic activity, PdZn-Co also exhibits remarkable stability and reusability (Fig. 3f). The recycled catalyst maintains the similar morphology and crystal structure (Fig. S11 in Supporting information).

To obtain an in-depth understanding of the relationship between structure and the photocatalytic activity, the DFT calculations of the charge density difference and adsorption energy (E_a) of Janus PdZn-Co are conducted out. The atomic electron density difference obviously presents the electrons of intermetallic PdZn are more delocalized than that of isolated Pd and Zn atom,

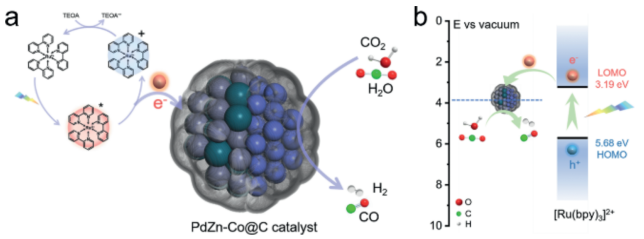

Fig. 4. (a) Scheme showing and (b) energy level diagram for the process.

whereas the electrons in metallic Co terminal are more clustered than that of isolated Co atoms (Figs. S12a and b in Supporting information). The electron density difference drives the electron migration from electron-rich PdZn terminal to electron-less Co terminal, which is in accord with the XPS results. The corresponding charge density difference directly displays the electron tend to concentrate on the Co terminal (Fig. S12c in Supporting information). The charge redistribution plays a vital role on the absorption of reactant molecule (Figs. S13–S15 in Supporting information). The electron-received Co terminal can facilitate Co sites coordinates with the electrophilic C atom of CO_2, the electron-donated PdZn center is easier to coordinate with nucleophilic O atoms of H_2O or C=O bonds [29]. The E_a for CO_2 molecule of metallic Co (111) is −0.544 eV. After introduction of PdZn, the Ea for CO_2 on metallic Co (111) increase to −1.034 eV. CO_2 adsorption measurements reveals the PdZn-Co shows a superior adsorption capacity than PdZn@C and Co@C (Fig. S16 in Supporting information). Furthermore, the interfaces of PdZn and Co terminal show a superior absorption performance of H_2O ($E_a = -0.979$ eV for H_2O) (Table S3 in Supporting information), as evidenced by contact angle test (Fig. S17 in Supporting information). On the other hand, the desorption energy for CO molecule of metallic of PdZn-Co (111) is similar as that of Co (111) (Fig. S18 in Supporting information). As a result, the enhanced absorption for CO_2 and H_2O facilitates photocatalytic H_2 evolution and CO_2 reduction.

The photogenerated electron transfer is essential for an excellent photocatalyst. The $[Ru(bpy)_3]Cl_2$ solution shows a strong emission peak around 610 nm under excited at 400 nm. After the addition of PdZn-Co catalyst, the intensity of PL peak is greatly diminished, which suggests the recombination of photogenerated charges substantially suppressed (Fig. S19a in Supporting information). The average emission lifetime of $[Ru(bpy)_3]Cl_2$ shortens after the addition of PdZn-Co catalyst (Fig. S19b in Supporting information). The declined PL intensity and the decrease of the lifetime indicate the catalyst can rapidly accept the photogenerated electron from the photosensitizer to participate the catalytic reaction. Furthermore, the band structure alignment of PdZn-Co and $[Ru(bpy)_3]Cl_2$ are investigated. The flat band potential of PdZn-Co is −0.63 eV (*vs.* NHE), determined by the Mott-Schottky analysis (Fig. S19c in Supporting information). The potential is lower than that of the lowest unoccupied molecular orbital (LUMO) of $[Ru(bpy)_3]Cl_2$ (−1.25 *vs.* NHE). As a result, the PdZn-Co catalyst can accept the electrons from the photosensitizer and transfer the electrons to activated CO_2 and H_2O for reduction. Based on the above analysis, the mechanism of the whole photocatalytic CO_2 and H_2O reduction process is introduced (Fig. 4). Firstly, the $[Ru(bpy)_3]^{2+}$ photosensitizer is excited under the visible light. The excited state $[Ru(bpy)_3]^{2+*}$ release electrons to PdZn-Co catalyst to form $[Ru(bpy)_3]^{3+}$. Then the $[Ru(bpy)_3]^{3+}$ is then reduced by TEOA. Finally, the CO_2 molecules are reduced to CO, simultaneously, the H_2O molecules are reduced to H_2 on the PdZn-Co catalyst. Overall, the PdZn-Co catalyst provides abundant active sites for effectively activate CO_2 and H_2O. Meanwhile, the introduction of PdZn-Co optimizes the photogenerated electron–hole separation and transfer, which accelerates the photoreduction process.

In summary, a Janus PdZn-Co catalyst is developed by calcined the Pd/IRMOF-3 (Zn, Co) precursor for photocatalytic reduction of CO_2 and H_2O to syngas (CO and H_2). The unique Janus structure modulates the charge redistribution between Co and PdZn terminals and enhances the absorption for CO_2 and H_2O, which promotes photocatalytic H_2 evolution and CO_2 reduction. The carbon shell effectively suppresses the metal core agglomeration and promotes the electron transmission from the photosensitizer to metallic active sites. The optimized PdZn-Co catalyst exhibits a superior photocatalytic CO production rate (20.03 μmol/h) and the H_2 generation rate (9.90 μmol/h). Meanwhile, the syngas ratio of CO/H_2 can be regulated from 2.93 to 2.02 by adjusting the proportion of Co and PdZn in the catalyst. The products of CO and H_2 with the applicable molar ratio can be further used as syngas raw to synthesize high value-added chemical feedstock.

Declaration of competing interest

The authors declare that they have no known competing financial interests or personal relationships that could have appeared to influence the work reported in this paper.

Acknowledgments

This work was supported by the National Natural Science Foundation of China (No. 51872025), the National Key R&D Program of China (No. 2021YFB3802200), Natural Science Foundation of Guangdong Province (No. 2220XCC061), the National Defense Basic Scientific Research (No. JCKY2021110B206), Scientific and Technological Innovation Foundation of Foshan (No. BK21BE008), Zibo Key Research and Development Program (No. 2020XCCG0036). The computing work was supported by USTB MatCom of Beijing Advanced Innovation Center for Materials Genome Engineering.

Supplementary materials

Supplementary material associated with this article can be found, in the online version, at doi:10.1016/j.cclet.2022.107798.

References

[1] J. Ran, M. Jaroniec, S.Z. Qiao, Adv. Mater. 30 (2018) 1704649.
[2] C. Cui, G. Li, Z. Tang, Chin. Chem. Lett. 32 (2021) 3307–3321.
[3] Z. Lei, Y. Xue, W. Chen, et al., Adv. Energy Mater. 8 (2018) 180157.
[4] A.M. Bahmanpour, M. Signorile, O. Kröcher, Appl. Catal. B: Environ. 295 (2021) 120319.
[5] X. Wang, Z. Wang, Y. Bai, et al., J. Energy Chem. 46 (2020) 1–7.
[6] S.W. Kim, M. Park, H. Kim, et al., Appl. Catal. B: Environ. 200 (2017) 265–273.
[7] G. Si, X. Kong, T. He, et al., Chin. Chem. Lett. 32 (2021) 918–922.
[8] M. Aresta, A. Dibenedetto, A. Angelini, Chem. Rev. 114 (2014) 1709–1742.
[9] K. Cao, Y. Ji, S. Bai, et al., J. Mater. Chem. A 9 (2021) 18349–18355.
[10] H. Huang, R. Shi, Z. Li, et al., Angew. Chem. Int. Ed. 61 (2022) e202200802.
[11] X. Chang, T. Wang, J. Gong, Energy Environ. Sci. 9 (2016) 2177–2196.
[12] Z. Wang, J. Yang, J. Cao, et al., ACS Nano 14 (2020) 6164–6172.
[13] L. Wang, W. Zhang, X. Zheng, et al., Nat. Energy 2 (2017) 869–876.
[14] L. Liang, X. Li, J. Zhang, et al., Nano Energy 69 (2020) 104421.
[15] W. Liao, W. Chen, S. Lu, et al., ACS Appl. Mater. Interfaces 13 (2021) 38239–38247.
[16] S. Wang, Z. Ding, X. Wang, Chem. Commun. 51 (2015) 1517–1519.
[17] M. Jiang, Y. Gao, Z. Wang, Z. Ding, Appl. Catal. B: Environ. 198 (2016) 180–188.
[18] J. Zhang, Y. Wang, H. Wang, D. Zhong, T. Lu, Chin. Chem. Lett. 33 (2022) 2065–2068.
[19] K. Zhao, S. Zhao, C. Gao, et al., Small (2018) e1800762.
[20] L. Wang, J. Wan, Y. Zhao, N. Yang, D. Wang, J. Am. Chem. Soc. 141 (2019) 2238–2241.
[21] C. Gao, Q. Meng, K. Zhao, et al., Adv. Mater. 28 (2016) 6485–6490.
[22] W. Chen, B. Han, C. Tian, et al., Appl. Catal. B: Environ. 244 (2019) 996–1003.
[23] C. Gao, S. Chen, Y. Wang, et al., Adv. Mater. 30 (2018) e1704624.
[24] S. Wang, B.Y. Guan, X.W. Lou, Energy Environ. Sci. 11 (2018) 306–310.
[25] B. Li, F. Wei, B. Su, et al., Mater. Today Energy 24 (2022) 100943.
[26] L. Yang, L. Li, P. Xia, et al., Chem. Commun. 57 (2021) 11629–11632.
[27] B. Liu, H. Zhou, H. Jin, et al., Chin. Chem. Lett. 32 (2021) 535–538.
[28] S. Wan, J. Wu, D. Wang, et al., Chin. Chem. Lett. 32 (2021) 816–821.
[29] Y. Xi, Y. Zhang, X. Cai, et al., Appl. Catal. B: Environ. 305 (2022) 121069.